Design and analysis of radomes

for Microstrip Patch Antenna at 6 GHz

Anvit Navin Khade

Design and analysis of radomes

for Microstrip Patch Antenna at 6 GHz

Krittika Summer Project
6.0

Author:	Anvit Navin Khade
Student ID:	23b1828
Supervisor:	Arjun Ghosh
Facilitator:	Aditi Singh
Project duration:	May 2025 – July 2025

Cover image:	Scott Noble; simulation data, d'Ascoli et al. 2018
Template style:	Thesis style by Richelle F. van Capelleveen
Template licence:	Licenced under CC BY-NC-SA 4.0

Indian Institute of Technology Bombay, Powai - 400076

Abstract

Radio-frequency (RF) and higher-frequency astronomy experiments are becoming increasingly vital for advancing our understanding of the universe. These observations, spanning from centimeter to millimeter wavelengths, provide key insights into early-universe physics, including the thermal evolution and the era of the Cosmic Microwave Background (CMB). To minimize thermal noise and enhance sensitivity, antennas operating in these regimes are often cryogenically cooled and housed within vacuum environments. Radome structures are used to maintain these vacuums while shielding the antennas from external elements. However, radomes can adversely affect the antenna's performance by altering its radiation pattern and introducing signal attenuation. This issue becomes more pronounced at lower RF frequencies, where the required radome thickness increases, further affecting signal fidelity. In this study, we design and simulate various RF antenna systems enclosed in multiple radome configurations. Through systematic analysis, we evaluated the effects of different materials, thicknesses, and geometrical arrangements on beam distortion and signal loss. The goal is to develop optimized radome solutions that ensure high observational precision while maintaining structural integrity and thermal isolation. Nabi et al. (2024)

Contents

1. Introduction to Antennas

Since the pioneering work of Hertz and Marconi, antennas have become indispensable components of modern life, embedded in homes, vehicles, satellites, and even personal devices. Despite their vast diversity in shape, size, and application, all antennas operate based on fundamental electromagnetic principles. Their designs range from simple to highly complex geometries. Antennas can function individually or as part of arrays and are used across a wide spectrum of applications, including broadcasting, radar, navigation, satellite communication, remote sensing, and deep space exploration. With the rapid growth in wireless technologies, antenna development continues to be a crucial and evolving field.

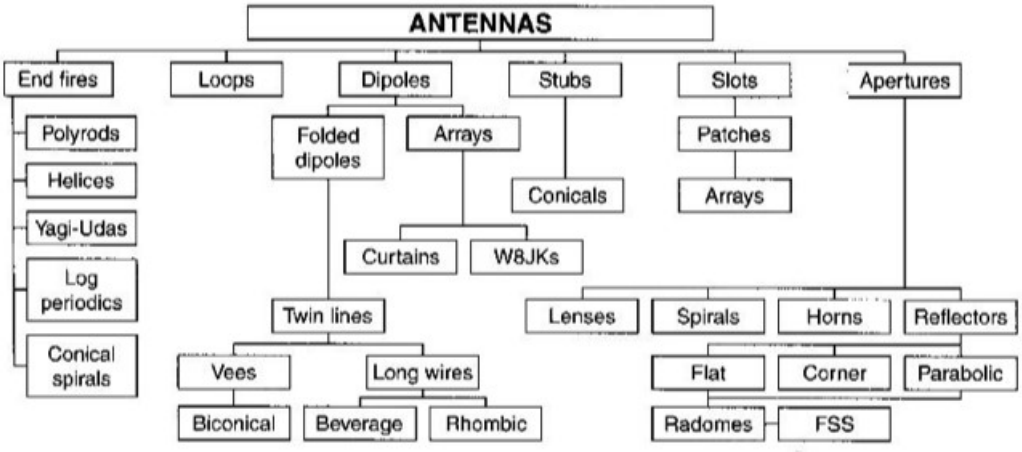

Figure 1.1: *Family of Antennas divided into six broad categories Kraus et al. (2010)*

1.1 Microstrip Patch antenna

Figure 1.2: *Patch antennas are provided for receiver and transmitter radio equipment for CubeSats as well as for other small satellites. cubsesat (2023)*

Patch antennas are low-profile antennas that consist of a flat conductive patch mounted over a ground plane, separated by a dielectric substrate. The patch can have various shapes with rectangular and circular being the most common.

Patch antennas are widely used in modern communication systems due to their compact size, ease of fabrication, and ability to conform to curved surfaces. They are ideal for applications such as mobile devices, satellites, GPS, and aircraft, where space and weight are critical.

Microstrip antennas began receiving significant attention in the 1970s, though their origin dates to 1953 with a 1955 patent. They consist of a thin metallic patch placed a small fraction of a wavelength above a ground plane, separated by a dielectric substrate. The patch is designed to radiate broadside by selecting the appropriate excitation mode. End-fire radiation is also possible with different modes. For rectangular patches, the length typically lies between lambda/3 and lambda/2. Balanis (2016) The substratesates have dielectric constants between 2.2 and 12. Low-dielectric, thick substrates provide higher efficiency and broader bandwidth but require larger elements. High-dielectric, thin substrates are preferred in microwave circuits for compact size and minimized radiation, but they reduce efficiency and bandwidth. Therefore, antenna and circuit design often require compromise

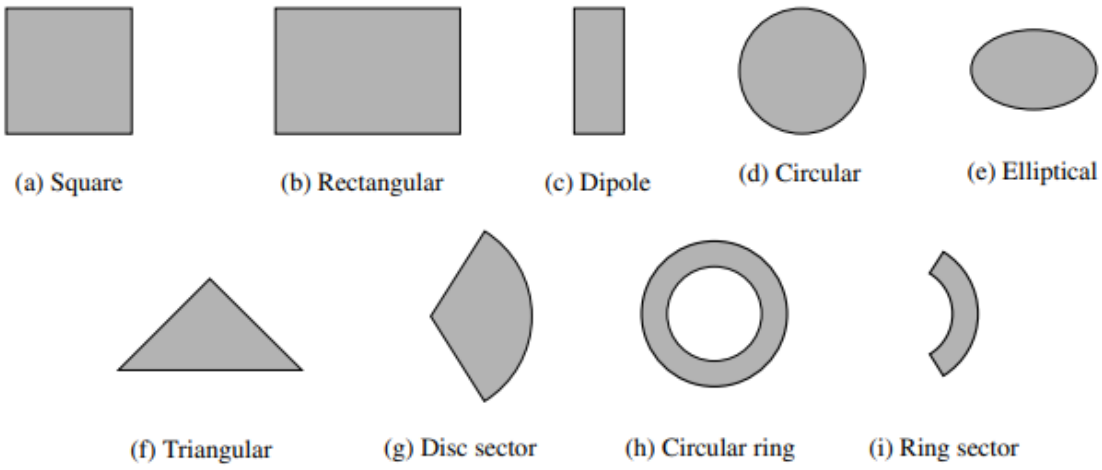

Figure 1.3: *Representative shapes of microstrip patch elements Balanis (2016)*

The patch and feed lines are usually photoetched on the substrate. Common patch shapes include square, rectangular, dipole (strip), circular, elliptical, and triangular, with the first four being most used due to ease of analysis and good radiation properties. Dipole patches offer large bandwidth and compactness, making them suitable for arrays. Both linear and circular polarizations are achievable with single elements or arrays. Arrays may also enable scanning and increased directivity.

Microstrip antennas have several operational disadvantages, including low efficiency, low power handling, high quality factor (often over 100), poor polarization purity, poor scan performance, spurious feed radiation, and very narrow bandwidth—typically a fraction to a few percent. Although narrow bandwidths are desirable in some applications like government security systems, performance can be improved by increasing substrate height, which boosts efficiency (up to 90% excluding surface waves) and bandwidth (up to 35%). However, this also introduces surface waves that degrade the radiation pattern and polarization due to scattering at discontinuities. Surface waves can be eliminated using cavities, and stacking elements can also increase bandwidth. Balanis (2016)

1.2 Structure of MSPA

Patch Antenna or Microstrip Antenna comprises of a patch, substrate and ground plane. Such antennas are useful in various aspects of Radio Astronomy.

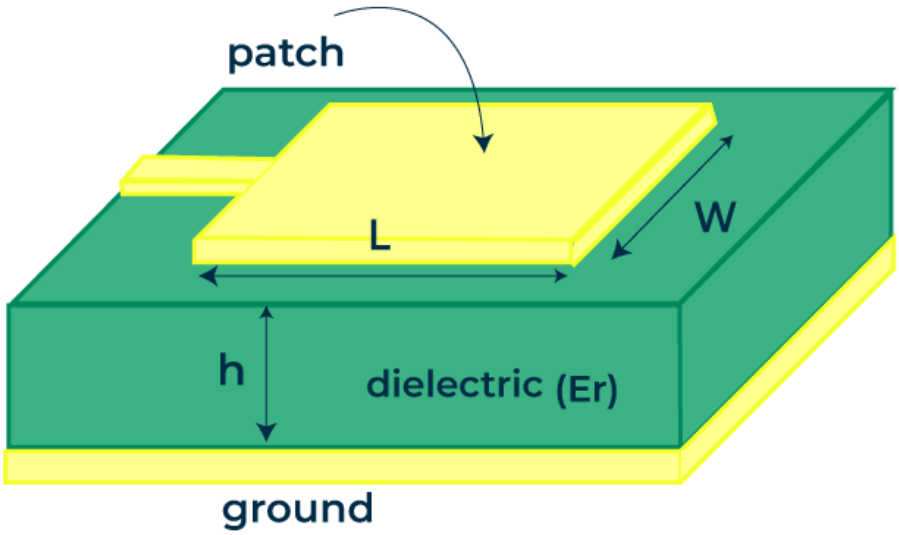

Figure 1.4: *Representative shapes of microstrip patch elements. gee (2024)*

Structure of a patch antenna:

- Patch (Radiating Element): A rectangular metallic layer, typically made of copper, this part radiates EM energy into free space.
- Ground plane: A large metallic sheet beneath the substrate. Acts as a reference point for the radiating patch and reflects energy to aid radiation.
- Substrate: An insulating material (e.g., FR4, RT Duroid) placed between the patch and ground plane. Determines the antenna's electrical characteristics, such as impedance and bandwidth.
- Feed line: A conducting strip that delivers RF power to the patch. In edge-fed designs, it connects directly to the edge of the patch where the input impedance is higher. Edge feed meaning it directly feeds to the edge of the patch.
- Inset cut: A notch or cut in the patch at the feed point. It is a technique used to match the input impedance of the antenna (typically 50 ohms) with that of the feed line. Werfelli et al. (2016)

1.3 Feeding Methods for Microstrip Antennas

There are several configurations used to feed microstrip antennas, with the four most popular being: microstrip line, coaxial probe, aperture coupling, and proximity coupling. These are shown below.

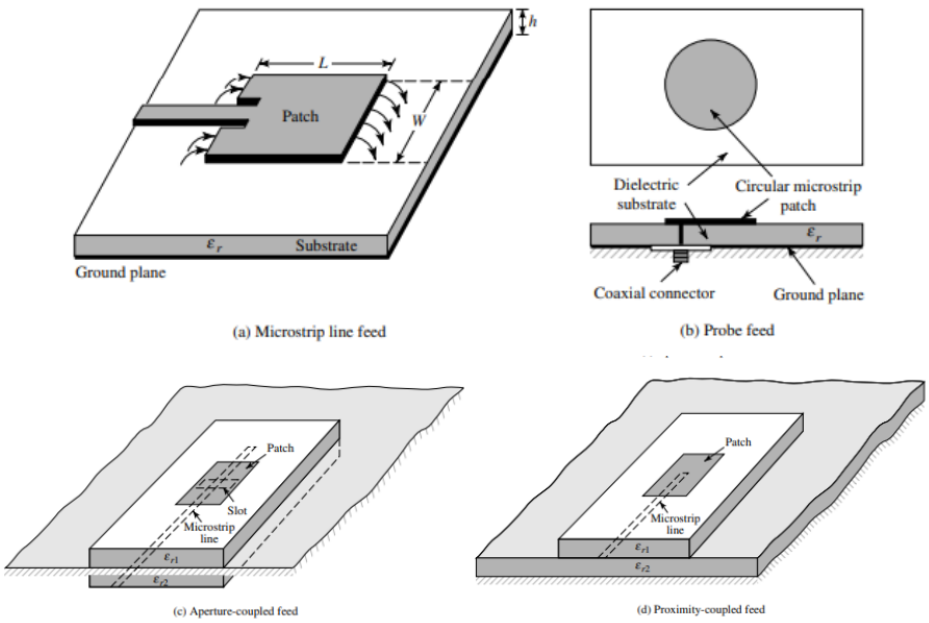

Figure 1.5: *Popular feeding methods for microstrip antennas: (a) microstrip line, (b) coaxial probe, (c) aperture coupling, and (d) proximity coupling. Balanis (2016)*

1. Microstrip Line Feed: This method uses a narrow conducting strip connected directly to the patch. It is easy to fabricate and match (by controlling the inset position) and is simple to model. However, it suffers from increased surface wave excitation and spurious radiation with thicker substrates, limiting bandwidth to 2–5%.

2. Coaxial Probe Feed: The inner conductor of the coaxial cable connects to the patch, and the outer conductor to the ground. It offers low spurious radiation and good matchability, but has narrow bandwidth and becomes difficult to model with thicker substrates ($h > 0.02\lambda_0$). Both this and the microstrip feed can produce cross-polarized radiation due to their asymmetry.

3. Aperture-Coupled Feed: This method uses two substrates separated by a ground plane with a slot. The feed line on the lower substrate couples energy through the slot to the patch on the upper substrate. It allows independent optimization of the feed and radiating element and reduces interference, improving polarization purity. Though harder to fabricate and offering narrow bandwidth, it is easier to model. Matching can be achieved by adjusting slot dimensions and feed line width.

4. Proximity-Coupled Feed: This contactless method provides the highest bandwidth (up to 13%), with low spurious radiation and moderate modeling complexity. It is harder to fabricate, but the feeding stub length and patch width-to-line ratio can be tuned for impedance matching.

2. Design of a 6 GHz MSPA

2.1 Calculating dimesnions of the antenna

2.1.1 Given Initial parameters

Operating Frequency: 6 GHz
Dielectric Material: FR4 Epoxy
Dielectric Constant, ε_r: 4.4
Substrate Height, h: 1.6 mm

2.1.2 Calculated Parameters

Kumar et al. (2021)

1. Width of the Patch W

$$W = \frac{c}{2f_0}\sqrt{\frac{2}{\varepsilon_r + 1}} = \frac{3 \times 10^8}{2 \times 6 \times 10^9}\sqrt{\frac{2}{4.4 + 1}} = 15.215 \text{ mm}$$

2. Effective Dielectric Constant ε_{eff}

$$\varepsilon_{\text{eff}} = \frac{\varepsilon_r + 1}{2} + \frac{\varepsilon_r - 1}{2}\left(\frac{1}{\sqrt{1 + 12\frac{h}{W}}}\right)$$

$$\varepsilon_{\text{eff}} = \frac{4.4 + 1}{2} + \frac{4.4 - 1}{2}\left(\frac{1}{\sqrt{1 + 12 \cdot \frac{1.6}{15.215}}}\right) = 3.830$$

3. Length of the Patch L

$$L = \frac{c}{2f_0\sqrt{\varepsilon_{\text{eff}}}} - 0.824 \cdot \frac{(\varepsilon_{\text{eff}} + 0.3)\left(\frac{W}{h} + 0.264\right)}{(\varepsilon_{\text{eff}} - 0.258)\left(\frac{W}{h} + 0.8\right)}$$

$$L = \frac{3 \times 10^8}{2 \times 6 \times 10^9 \cdot \sqrt{3.830}} - 0.824 \cdot \frac{(3.830 + 0.3)(\frac{15.215}{1.6} + 0.264)}{(3.830 - 0.258)(\frac{15.215}{1.6} + 0.8)} = 11.329 \text{ mm}$$

4. Input Impedance Z_{in}

$$Z_{\text{in}} = 90\left(\frac{\varepsilon_r^2}{\varepsilon_r - 1}\right)\left(\frac{L}{W}\right)^2$$

$$Z_{\text{in}} = 90 \cdot \left(\frac{4.4^2}{4.4 - 1}\right) \cdot \left(\frac{11.329}{15.215}\right)^2 = 284.124\,\Omega$$

5. Transmission Line Width W_0

Given that the desired impedance is 50, and using standard microstrip formulas:

$$W_0 = 2.377\,\text{mm} \quad \text{(calculated using line impedance equations)}$$

6. Inset Spacing S

$$S = \frac{1}{2}W_0 = \frac{1}{2} \cdot 3.37 = 1.685\,\text{mm}$$

7. Substrate and Ground Plane Dimensions (6h Rule)

To minimize edge effects and improve radiation performance, the substrate and ground plane dimensions are extended by $3h$ on each side (total $6h$):

$$W_{\text{sub}} = w + 6h \quad \text{and} \quad L_{\text{sub}} = l + 6h$$

Where:

- $w = 15.215\,\text{mm}$ (Patch width)
- $l = 11.329\,\text{mm}$ (Patch length)
- $h = 1.6\,\text{mm}$ (Substrate height)

$$W_{\text{sub}} = 15.215 + 6 \times 1.6 = 24.815\,\text{mm}$$
$$L_{\text{sub}} = 11.329 + 6 \times 1.6 = 20.129\,\text{mm}$$

2.2 CAD Modelling and Simulation of the 6 GHz MSPA

A CAD model was created in ANSYS HFSS by defining variable dimensions, for convenient parametric optimization discussed in the later stages.

2.2.1 Simulation Configuration

Patch and Ground: Perfect Electric Conductor (PEC), modeled using copper
Substrate: FR4 Epoxy with $\varepsilon_r = 4.4$
Excitation: Lumped Port (or Wave Port) with 50 Ω impedance
Radiation Box: $\lambda/4$ distance from the patch in all directions
Frequency Sweep: 1 GHz to 12 GHz with 733 points
Solution Frequency: 6 GHz

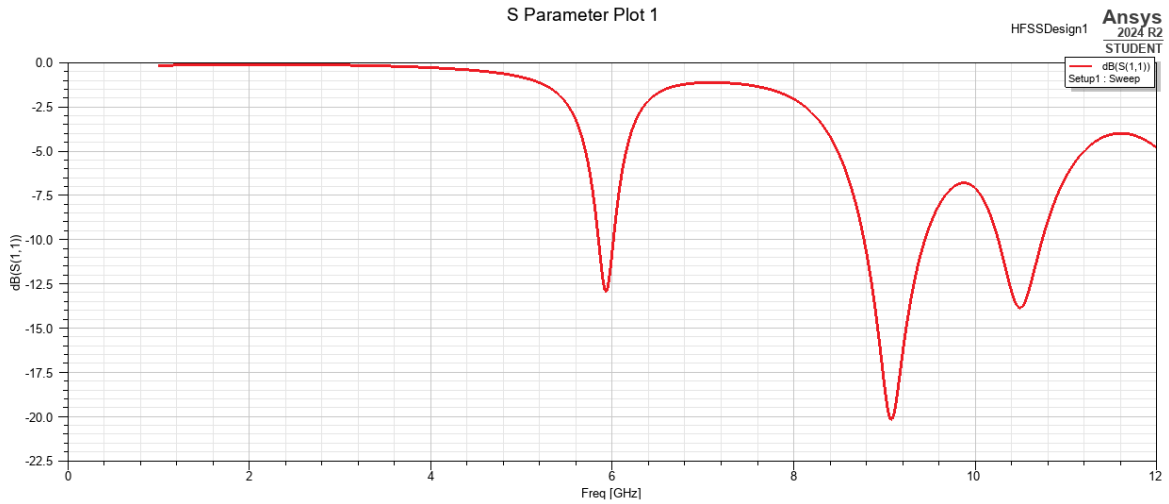

Figure 2.1: Initial S11 plot using dimensions from analytical calculations. Note: the antenna does not resonate sharply at 6 GHz.

2.2.2 Parametric Sweep

A parametric sweep was conducted for the inset depth, ranging from 2 mm to 4 mm in 0.4 mm steps. The optimal return loss was observed at an inset depth of 2.9 mm and an inset width of 1.5 mm.

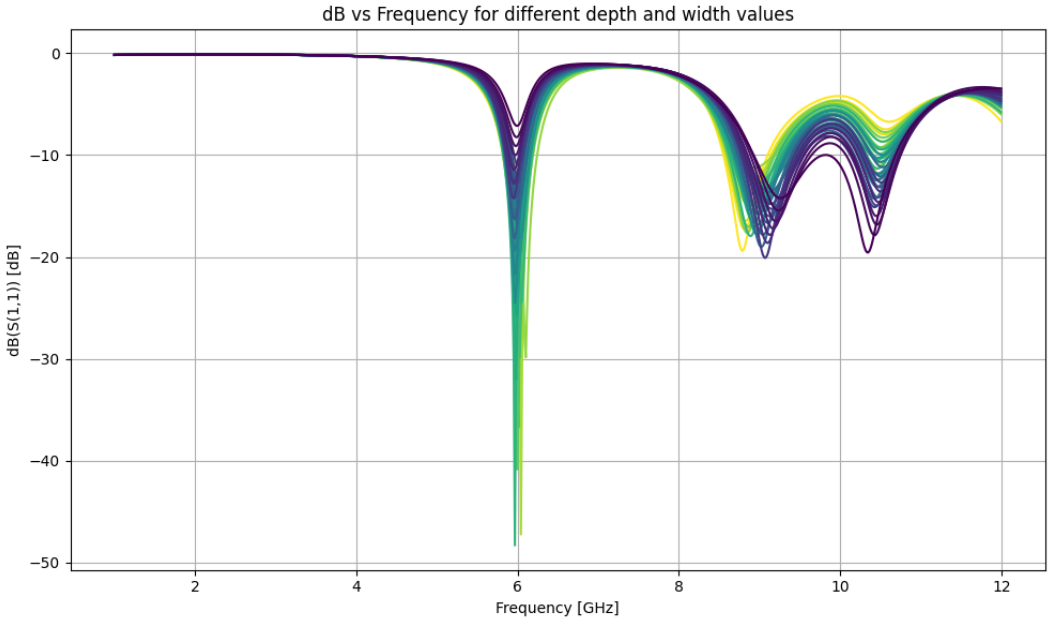

Figure 2.2: Parametric sweep of inset cut dimensions to optimize impedance matching.

2.3 Simulation Results

2.3.1 S11 (Return Loss)

The simulated S11 parameter demonstrates excellent resonance and impedance matching:

- **Minimum S11:** −48.2 dB at 5.99 GHz (excellent matching)
- **Bandwidth (S11 < −10 dB):** 5.78 GHz to 6.22 GHz, yielding a bandwidth of approximately 440 MHz
- **At 6.01 GHz:** Return loss of −46.7 dB implies less than 0.002% of input power is reflected, with over 99.998% radiated

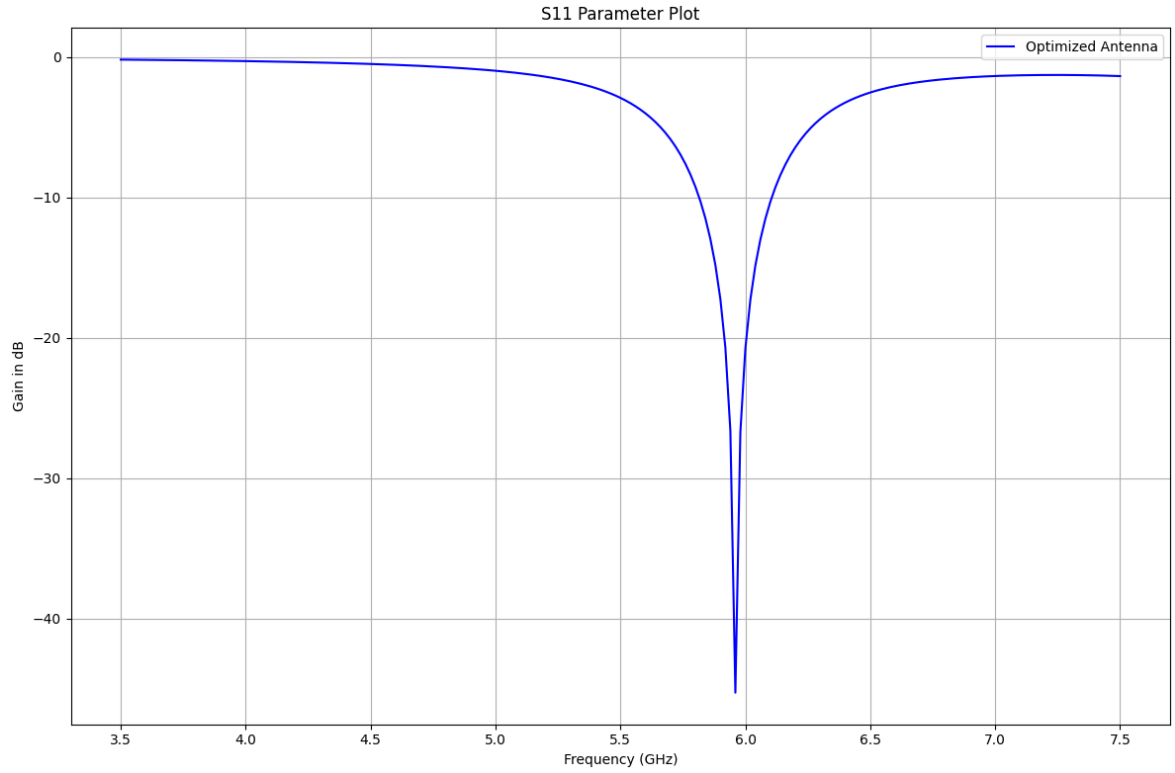

Figure 2.3: *Optimized S11 parameter plot of Microstrip plot antenna after parametric sweep of inset cut.*

2.3.2 Co-polarization and Cross-polarization of E-Plane

The E-plane radiation pattern was analyzed to evaluate the antenna's polarization performance. Co-polarization refers to the intended polarization component (aligned with the desired field), while cross-polarization represents the undesired orthogonal component.

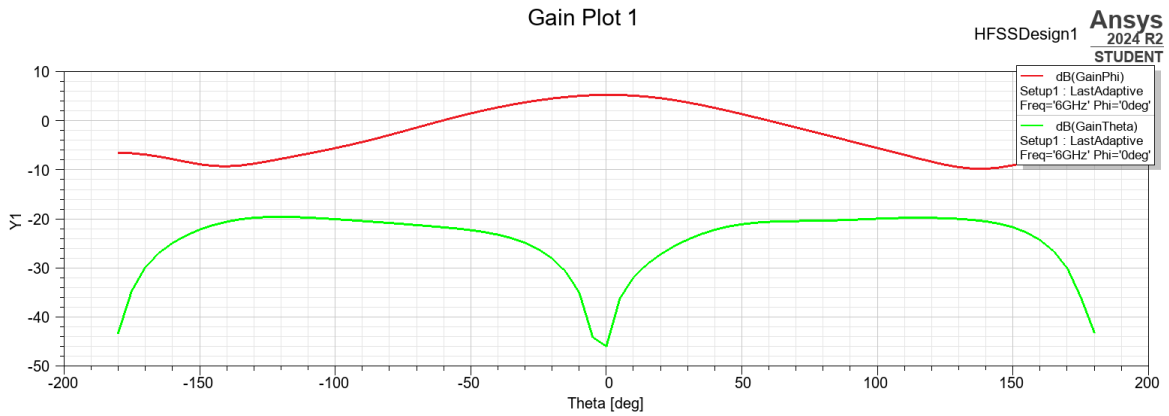

Figure 2.4: *Co-polarization and cross-polarization comparison in the E-plane at 6 GHz.*

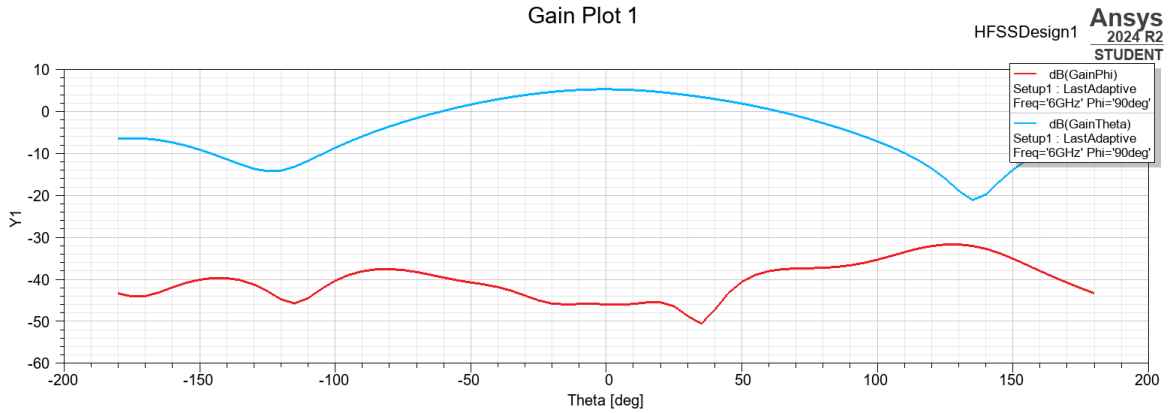

Figure 2.5: *Co-polarization and cross-polarization comparison in the H-plane at 6 GHz.*

The plot in Figure 3.3 shows a clear separation between the co-polarized and cross-polarized components at the target frequency of 6 GHz. This wide separation implies excellent polarization purity, indicating that the antenna efficiently radiates the desired polarization with minimal interference from the orthogonal component. Such performance is essential for reducing signal distortion and improving communication system reliability.

3. Radome

In radio astronomy, antennas are used to detect extremely weak electromagnetic signals across a broad frequency spectrum, from centimeter to sub-millimeter wavelengths. These antennas are often part of highly sensitive cryogenic systems designed to minimize front-end noise and maximize signal fidelity. To preserve this sensitivity, it is essential to house such antennas within enclosures that protect against environmental effects while introducing minimal electromagnetic distortion—this is the role of a radome.

Radomes are specialized enclosures that are transparent to electromagnetic waves and serve multiple critical functions in radio astronomy. They shield antennas and frontend electronics from weather, dust, and temperature fluctuations, while also enabling the maintenance of a vacuum environment crucial for cryogenically cooled components.

Figure 3.1: *Naval radomes for radar systems used in military grade application*

This work aims to investigate how the choice of material, structural geometry, and radome placement affect signal transmission characteristics. The goal is to identify configurations that preserve the integrity of the antenna's beam pattern, reduce power loss, and maintain high sensitivity, particularly in the context of cryogenic receiver systems and precision scientific measurements.

3.1 Understanding Dielectric Constant and Loss Tangent

To understand electromagnetic wave propagation through radome materials, it is essential to consider the material's constitutive parameters: permittivity, permeability, and conductivity. These properties define how the material interacts with incident electromagnetic waves. For most radome applications, non-magnetic dielectric materials are used, with relative permeability $\mu_r = 1$ and negligible conductivity.

A key parameter in material selection is the dielectric constant (also known as relative permittivity, ε_r or Dk), which affects both reflection and refraction of waves at the material boundaries. A mismatch between the Dk of the radome and air can cause signal fading due to boundary reflections or internal multi-path reflections.

Dielectric loss, quantified by the loss tangent $\tan(\delta)$, characterizes the material's inherent dissipation of electromagnetic energy. Both the dielectric constant and loss tangent should ideally be low to ensure minimal effect on antenna performance. While a Dk close to 1 is desirable (as in free space), practical radome materials typically have higher values due to mechanical, cost, and environmental considerations.

3.2 Impedance Mismatch at Radome Boundaries

When an electromagnetic wave crosses from one medium to another with different dielectric properties, impedance mismatch occurs at the boundary, leading to partial reflection and transmission of the wave. This boundary mismatch can be characterized using reflection (Γ) and transmission (τ) coefficients:

$$\Gamma = \frac{E_r}{E_i}, \quad \tau = \frac{E_t}{E_i}$$

where E_i, E_r, and E_t are the incident, reflected, and transmitted electric field magnitudes, respectively.

At the radome–air interfaces, these mismatches result in multiple internal reflections that accumulate and can distort the outgoing signal. Free-space impedance is approximately 377 Ω, while inside a dielectric material, it becomes $377/\sqrt{\varepsilon_r}\ \Omega$. This discontinuity at both the air–radome and radome–air interfaces generates complex reflection behavior, contributing to insertion loss and phase distortion.

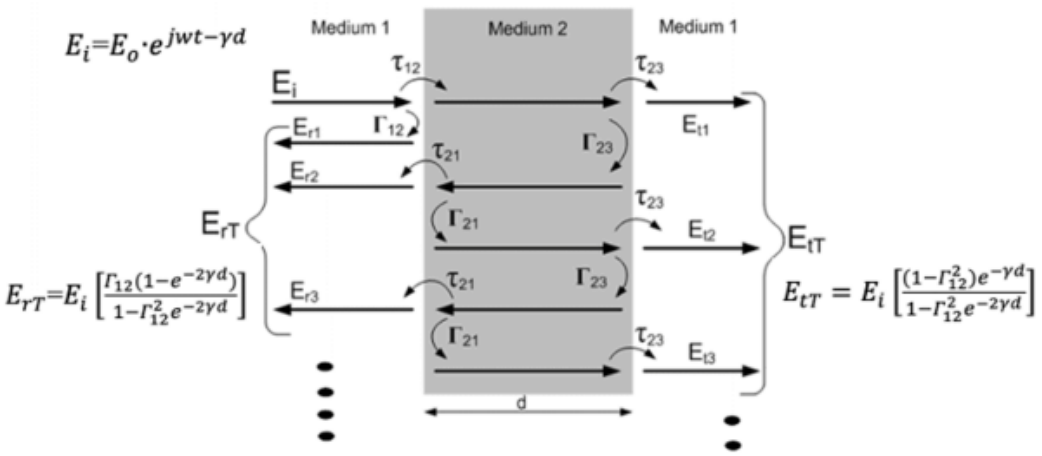

Figure 3.2: Multiple Reflections at Boundaries of Dielectric Mediums Kumar et al. (2021)

3.3 Radome Parameter Derivation

This section presents the theoretical background and derivations related to the electromagnetic performance of radomes in radio astronomy systems. It includes discussions on material selection, impedance mismatch, wave behavior, and geometric design strategies, all aimed at minimizing signal degradation through the radome.

3.3.1 Transmitted and Reflected Waves for a Radome

We consider a symmetric dielectric slab setup, where an electromagnetic wave travels from Medium 1 into a dielectric slab (Medium 2) of thickness d, and then exits back into Medium 1. This structure is symmetric in impedance mismatch and results in multiple reflections inside the slab. The goal is to compute the total transmitted and reflected electric fields.

Incident and Propagation Parameters

- Medium 1 $\rightarrow$ Medium 2 (thickness d) $\rightarrow$ Medium 1
- Incident field: $E_i = E_0 e^{j\omega t - \gamma d}$, where $\gamma = \alpha + j\beta$
- Reflection and transmission coefficients at both interfaces are equal:

$$\Gamma_{12} = \Gamma_{23} = \Gamma, \quad \tau_{12} = \tau_{23} = \tau$$

Transmitted Field Derivation

The total transmitted field is a summation of all transmitted components after multiple reflections within the slab:

$$E_{tT} = E_i \cdot \tau^2 \cdot e^{-\gamma d} \sum_{n=0}^{\infty} \left(\Gamma^2 e^{-2\gamma d}\right)^n$$

$$E_{tT} = E_i \cdot \frac{\tau^2 e^{-\gamma d}}{1 - \Gamma^2 e^{-2\gamma d}}$$

Using the identity $\tau^2 = 1 - \Gamma^2$, this simplifies to:

$$\boxed{E_{tT} = E_i \cdot \frac{(1 - \Gamma^2) e^{-\gamma d}}{1 - \Gamma^2 e^{-2\gamma d}}}$$

Special Case: Constructive Interference

When $2\beta d = 2n\pi$, the internal reflections interfere constructively:

$$e^{-j2\beta d} = 1 \Rightarrow \text{Maximum transmission}$$

$$E_{tT} = E_i \cdot e^{-j\beta d}$$

Thus, the radome achieves near-perfect transmission (aside from a phase shift), even if each interface is reflective.

Reflected Field Derivation

Similarly, the reflected field is given by:

$$E_{rT} = E_i \cdot \Gamma + \tau^2 \cdot \Gamma \cdot e^{-2\gamma d} \sum_{n=0}^{\infty} \left(\Gamma^2 e^{-2\gamma d}\right)^n$$

$$E_{rT} = E_i \cdot \Gamma \cdot \left(1 + \frac{(1 - \Gamma^2) e^{-2\gamma d}}{1 - \Gamma^2 e^{-2\gamma d}}\right)$$

$$\boxed{E_{rT} = E_i \cdot \Gamma \cdot \frac{1 - e^{-2\gamma d}}{1 - \Gamma^2 e^{-2\gamma d}}}$$

Summary of Results

These equations model the behavior of electromagnetic waves in layered dielectric radome structures and are critical in optimizing thickness and material parameters for minimal reflection and maximum signal integrity.

3.3.2 Optimal Distance Between Antenna and Radome

One of the primary challenges in radome design is minimizing the impact of reflected waves from the inner surface of the radome back toward the antenna. If these reflected waves are not appropriately managed, they may destructively interfere with the original signal, causing distortion or signal degradation.

To ensure constructive interference between the forward-traveling wave and any reflected wave returning from the radome inner surface, the reflected wave must return *in phase* with the outgoing wave. This condition is satisfied when the round-trip distance equals an integer multiple of the free-space wavelength λ_0.

Phase Condition for Constructive Interference: Let,
D: distance between antenna and inner surface of the radome
λ_0: free-space wavelength
$n \in \mathbb{Z}^+$: positive integer
For constructive interference, the phase difference after a round trip must be:

$$2D = n\lambda_0 \quad \Rightarrow \quad D = \frac{n\lambda_0}{2}$$

$$\boxed{D = \frac{n\lambda_0}{2}, \quad n = 1, 2, 3, \ldots} \tag{3.1}$$

This expression gives the optimal separation distance between the antenna and radome. At these discrete spacings, any reflected wave arrives in phase with the transmitted wave, minimizing destructive interference and maximizing transmission efficiency.

3.3.3 Optimal Radome Wall Thickness

The thickness of the radome wall plays a critical role in determining the overall electromagnetic transparency of the radome structure. To ensure minimal reflection and maximal transmission, the radome wall should be designed such that its thickness corresponds to a condition of constructive interference for the wave propagating through it. This condition is met when the thickness is an integer multiple of half the wavelength inside the radome material:

Interference Condition in the Dielectric Medium: Let,
t_{optimum}: Optimal thickness of the radome wall
λ_m: Wavelength of the signal inside the radome material
$n \in \mathbb{Z}^+$: Positive integer

The constructive interference condition gives:

$$t_{\text{optimum}} = \frac{n\lambda_m}{2}$$

$$\boxed{t_{\text{optimum}} = \frac{n\lambda_m}{2}, \quad n = 1, 2, 3, \ldots} \tag{3.2}$$

Wavelength in the Dielectric
The wavelength inside the radome material is shorter than in free space and is given by:

$$\lambda_m = \frac{c}{f\sqrt{\varepsilon_r}}$$

where:
c: Speed of light in vacuum ($\approx 3 \times 10^8$ m/s)
f: Operating frequency
ε_r: Relative permittivity (dielectric constant) of the radome material

$$\boxed{\lambda_m = \frac{c}{f\sqrt{\varepsilon_r}}} \tag{3.3}$$

Final Expression
Substituting for λ_m in the optimal thickness equation:

$$\boxed{t_{\text{optimum}} = \frac{nc}{2f\sqrt{\varepsilon_r}}} \tag{3.4}$$

3.4 Errors Introduced by Flat Radome

Flat or rectangular radomes, though simple to fabricate, introduce angular-dependent errors due to varying electrical path lengths for incident electromagnetic waves at different angles.

Angle-Dependent Path Length
At boresight (normal incidence), the wave traverses the radome thickness directly, and when this thickness is optimized (e.g., $\lambda/2$), internal reflections cancel out due to destructive interference. This ensures minimal net reflection and optimal signal transmission.

However, for waves incident at higher grazing angles, the effective path length through the radome wall increases due to the oblique traversal. This increased path introduces phase mismatches, leading to constructive and destructive interference at unintended positions in the radiation pattern.

Phase Mismatch and Reflection Ripples
When the wall thickness is no longer exactly $\lambda/2$ due to the oblique angle, reflections at the radome interfaces are no longer out of phase. This causes:

- Multiple internal reflections
- Ripple effects in the antenna's radiation pattern
- Unwanted nulls and peaks

These artifacts distort the angular accuracy of received or transmitted signals, especially in radar and radio astronomy applications where precision is critical.

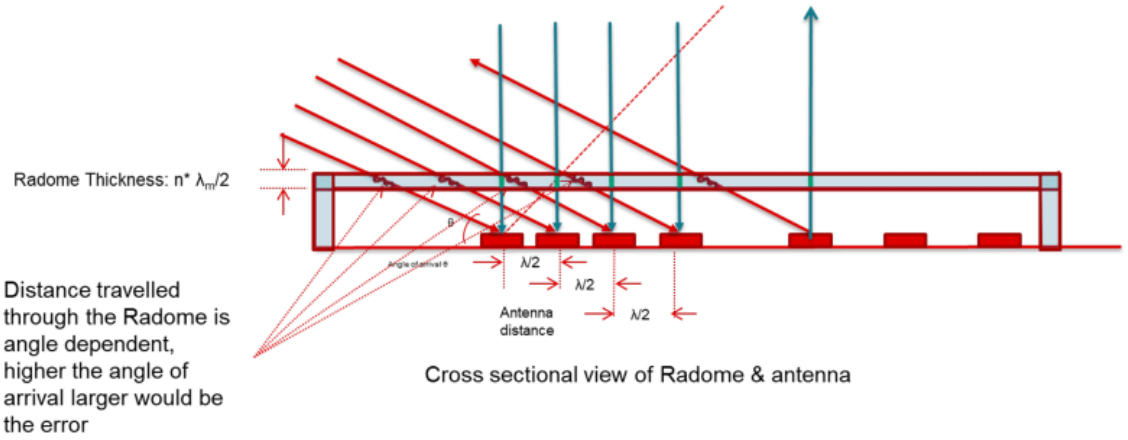

Figure 3.3: *Distance Traveled in Rectangular Radome Wall for Different Grazing Angles Kumar et al. (2021)*

Impact on Angle Estimation

The inconsistent phase shifts at higher incident angles result in:

- Degraded beamforming resolution
- Angle-of-arrival estimation errors
- Reduced sensitivity at the edges of the field of view

One way to minimize this angular dependency is by tapering the radome wall, making it thinner at larger field-of-view angles. While this can help equalize the electrical path across angles, it comes at the cost of structural strength and mechanical integrity.

4. HFSS Analysis of Radome

A flat radome configuration was designed as a planar enclosure using SolidWorks using the parameters calculated as per the previous section. Now we present simulation results illustrating the impact of a flat radome on the antenna's input matching and radiation characteristics. McCulloch et al. (2023)

4.1 Radome Geometry and Material Selection

A flat radome configuration was designed as a planar enclosure using the standard quarter-wave matching principle. The wall thickness was derived using:

$$t_{\text{optimum}} = n\frac{\lambda_0}{2\sqrt{\varepsilon_r}}, \tag{3.1}$$

where n is an integer, λ_0 is the free-space wavelength, and ε_r is the relative permittivity of the radome material.

To minimize multipath reflection and phase errors, the radome was placed at a distance from the antenna given by:

$$D_{\text{opt}} = n\frac{\lambda_0}{2} \tag{3.2}$$

Radome materials were chosen with low dielectric constant and low loss tangent, as shown in Table 4.1:

Table 4.1: *Typical Radome Materials*

Material	ε_r	tan δ
Polycarbonate	2.9	0.012
ABS	2.0–3.5	0.005–0.019
PTFE (Teflon)	2.0	<0.0002
Plexiglass	2.6	0.009

These structures were modeled in HFSS and placed around the antenna to assess changes in return loss, gain, and radiation patterns.

4.2 Simulation of Antenna–Flat Radome System

This section presents simulation results illustrating the impact of a flat radome on the antenna's input matching and radiation characteristics.

4.2.1 S_{11} Parameter Comparison

An overlay plot of the S_{11} parameter for the patch antenna with and without the radome is shown in Figure 4.1. The addition of the radome results in a slight degradation in return loss, but without causing noticeable impedance mismatch. Moreover, the observed gain drop is minimal and does not significantly impact the overall system performance.

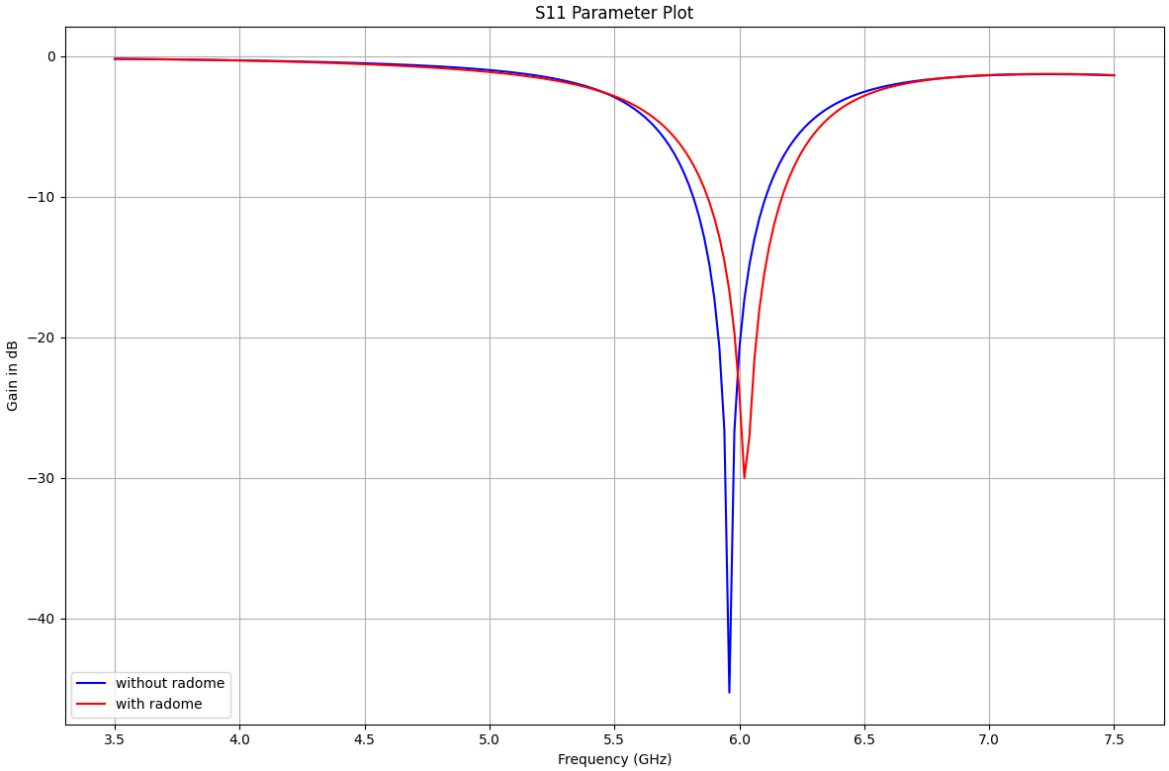

Figure 4.1: *S_{11} comparison of antenna with and without flat radome.*

4.2.2 E-Plane and H-Plane Radiation Patterns

Contrary to our expectations, the gain with radome is observed to be more in the zenith and nadir directions. This occurs because the radome introduces internal reflections that lead to constructive interference, slightly boosting gain at certain angles. However, in the absence of an external absorbing cover, a portion of the radiated energy is redirected into back lobes, ultimately reducing the effective forward gain despite local increases, and thus impacting the antenna's directional performance.

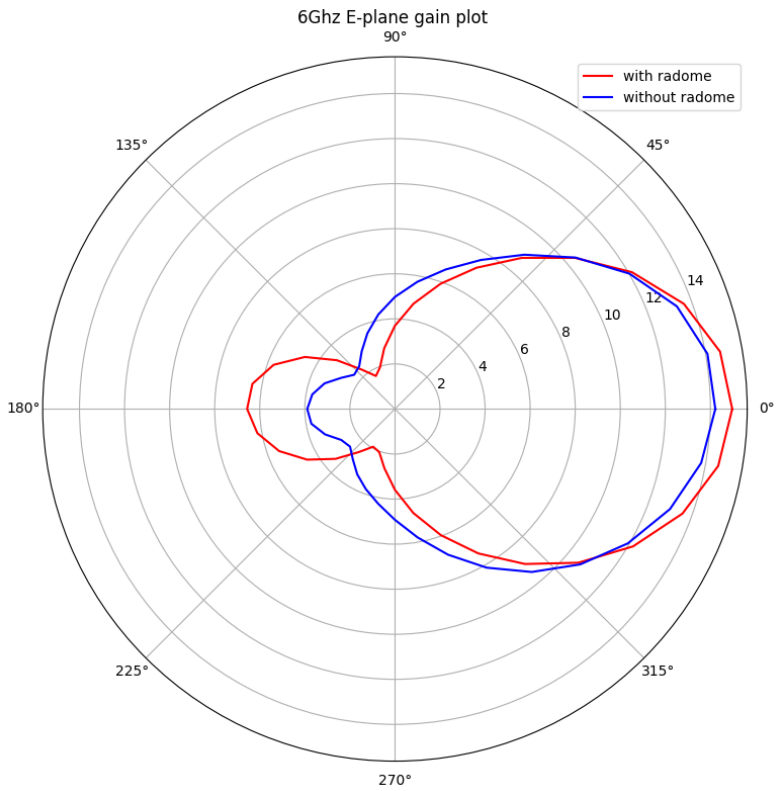

Figure 4.2: *E-plane 2D gain patterns with and without radome for 6Ghz frequency*

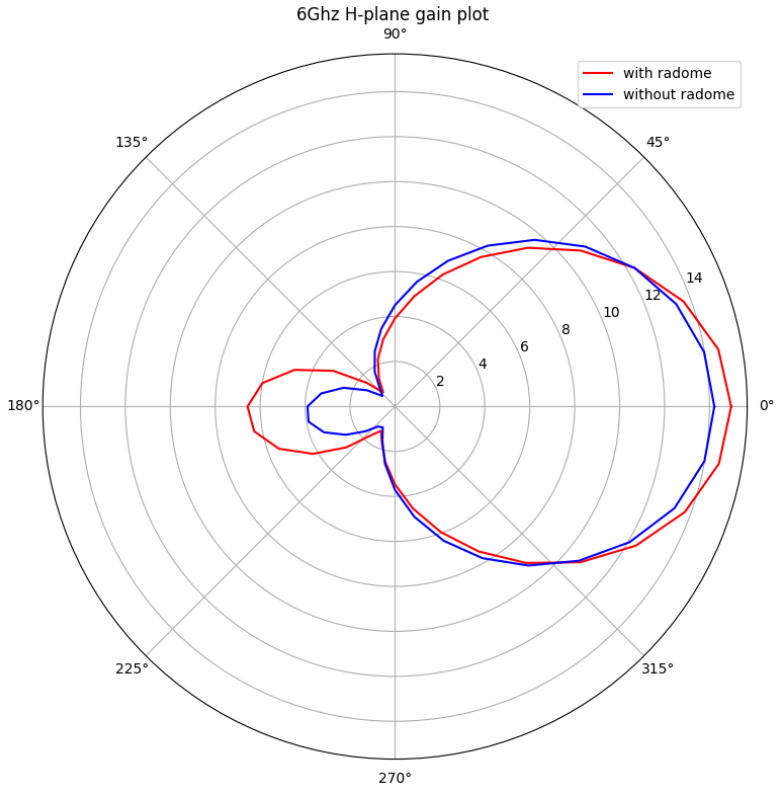

Figure 4.3: *H-plane 2D gain patterns with and without radome for 6Ghz frequency*

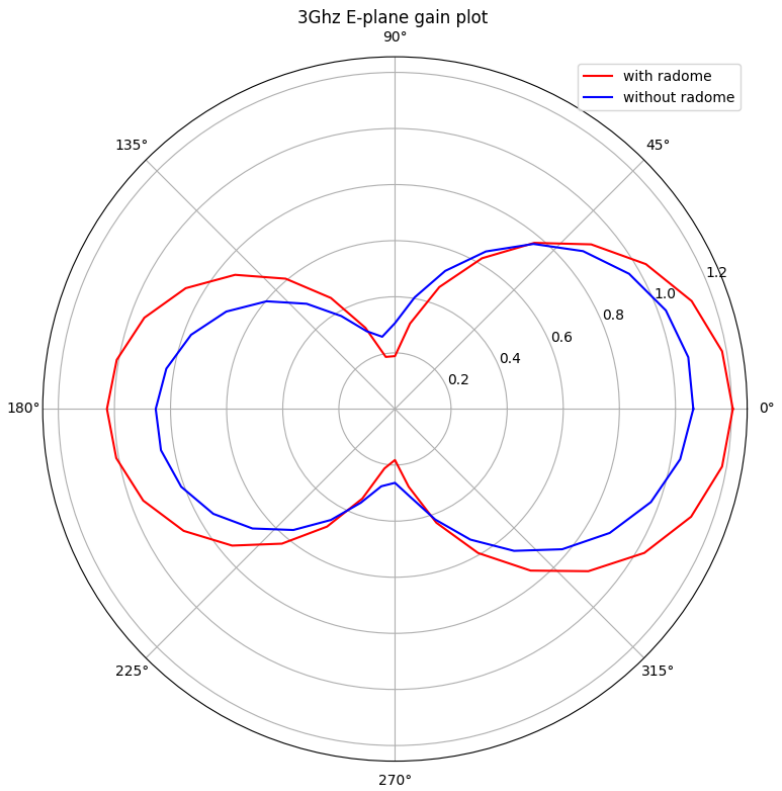

Figure 4.4: *E-plane 2D gain patterns with and without radome for 3Ghz frequency*

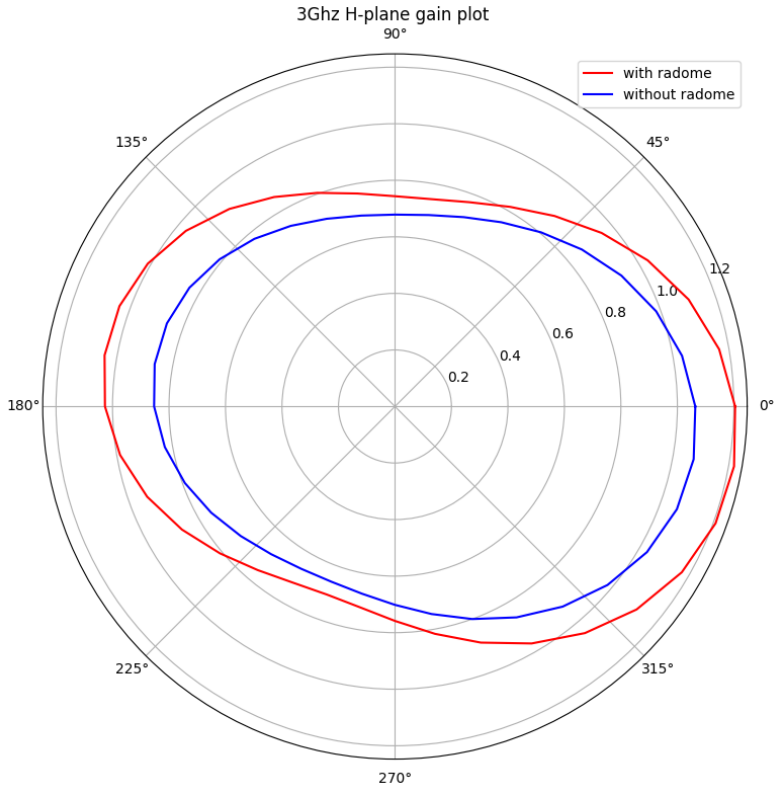

Figure 4.5: *H-plane 2D gain patterns with and without radome for 3Ghz frequency*

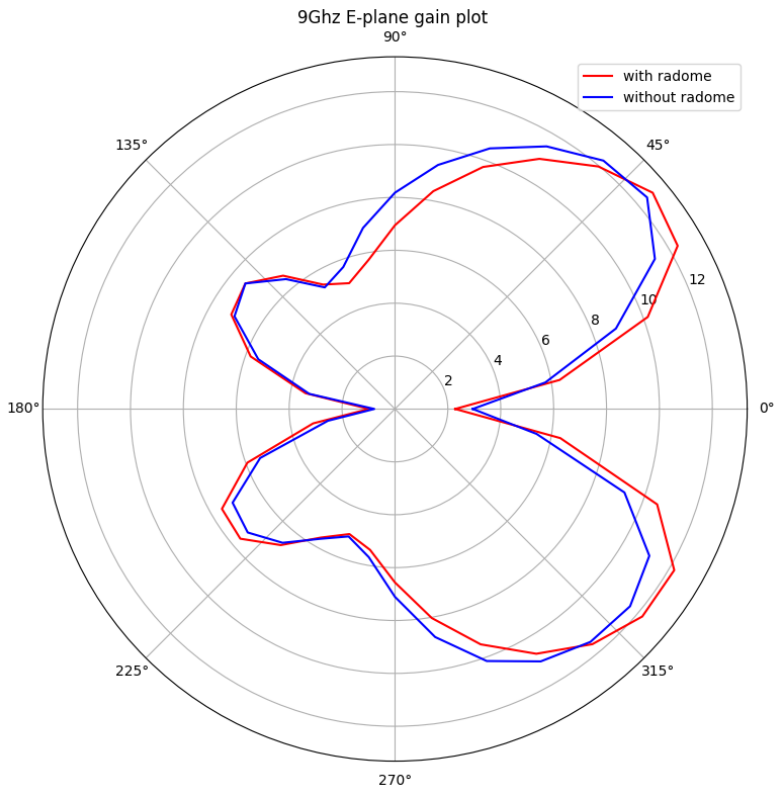

Figure 4.6: *E-plane 2D gain patterns with and without radome for 9Ghz frequency*

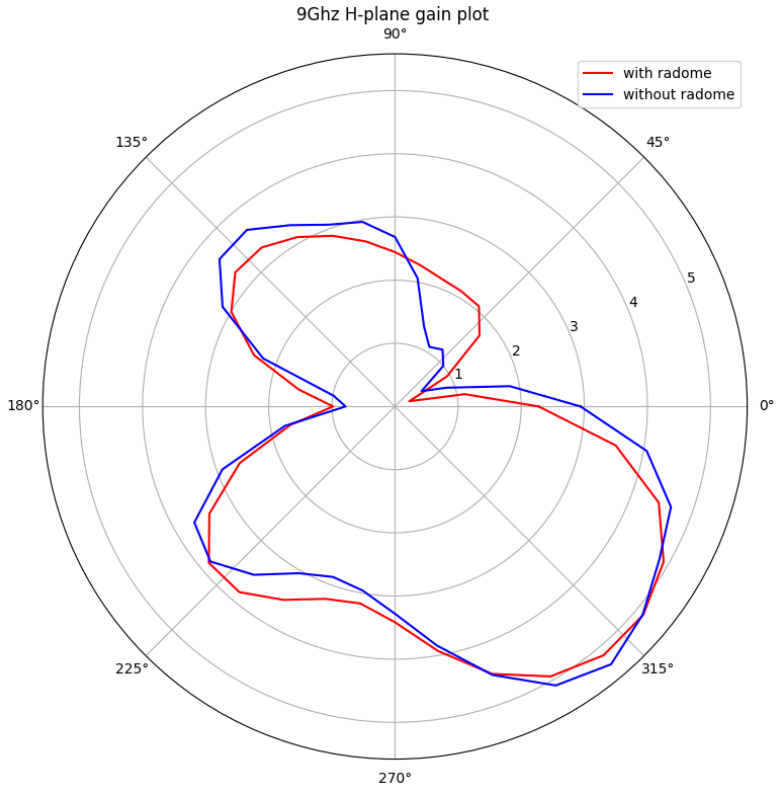

Figure 4.7: *H-plane 2D gain patterns with and without radome for 9Ghz frequency*

4.2.3 Parametric Sweep on Antenna–Radome Distance (d)

To analyze the optimal placement of the radome, a parametric sweep was conducted by varying the distance d between the antenna and the inner wall of the radome.

- The sweep results show that certain values of d lead to constructive interference and lower reflection, while others worsen performance due to phase mismatch.
- The optimal d occurs when the spacing equals an integral multiple of $\lambda_0/2$, as derived earlier:

$$d = n \cdot \frac{\lambda_0}{2}, \quad n = 1, 2, 3, \ldots$$

- This configuration minimizes standing wave formation due to internal reflections and results in improved S_{11} and radiation pattern symmetry.

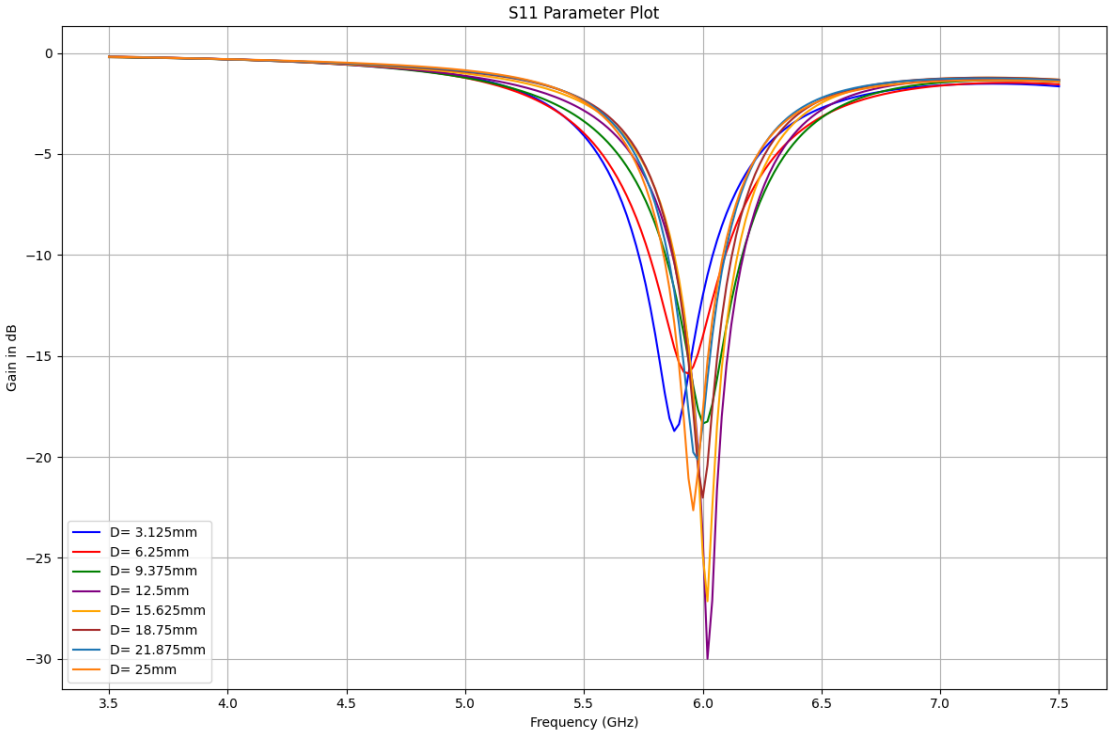

Figure 4.8: *Parametric Sweep on Antenna–Radome Distance*

5. Conclusion

In this report, a comprehensive design and simulation workflow was carried out for a 6GHz inset-fed microstrip patch antenna, optimized using theoretical formulations and HFSS simulations. The antenna's performance, including return loss and radiation characteristics, was validated and optimized using parametric sweeps.

Subsequently, the impact of introducing a flat dielectric radome was investigated. Although the radome resulted in minor constructive interference effects that slightly increased gain at the boresight and nadir, it also introduced increased back lobe radiation due to internal reflections. This caused a degradation in the front to back ratio, ultimately reducing the antenna's forward directivity.

Key design considerations such as radome thickness and antenna–radome spacing were theoretically derived and verified through simulation. The results confirm that optimal radome performance minimal reflection and maximal transmission can be achieved when the wall thickness is an integer multiple of half the wavelength in the radome material, and when the antenna to radome spacing also satisfies the half-wavelength condition in free space.

This study highlights the importance of carefully integrating radome design with antenna systems in radio astronomy and related RF applications, where both environmental protection and minimal electromagnetic interference are essential.

Bibliography

2024, labelled mspa antenna, https://www.geeksforgeeks.org/electronics-engineering/microstrip-patch-antenna/

Balanis, C. A. 2016, Antenna theory: analysis and design (John wiley & sons)

cubsesat, A. 2023, MSPA, https://www.satcatalog.com/component/patch-antenna/

Kraus, J. D., Marhefka, R. J., & Khan, A. S. 2010, Antennas and Wave Propagation, Tata McGraw Hills Publication

Kumar, C., Mohammed, H. U. R., & Peake, G. 2021, Texas Instruments Incorporated, US

McCulloch, M. A., D'Cruze, M., Grainge, K., Keith, M., & Melhuish, S. 2023, RAS Techniques and Instruments, 2, 432

Nabi, R., Wei-Jun, L., & Majeed, M. R. 2024, European Journal of Electrical Engineering and Computer Science, 8, 77

Werfelli, H., Tayari, K., Chaoui, M., Lahiani, M., & Ghariani, H. 2016, in 2016 2nd International Conference on Advanced Technologies for Signal and Image Processing (ATSIP), IEEE, 798–803